Military Technical College
Kobry El-Kobbah,
Cairo, Egypt.

18th International Conference on Applied Mechanics and Mechanical Engineering.

A NUMERICAL STUDY ON STEAM EJECTOR OPTIMUM PERFORMANCE

T. A. Ghonim[1], M. S. Farag[1] and A. S. Hegazy[2]

ABSTRACT

The present paper introduces a numerical study on the optimum performance of steam ejector at constant pressure ratio. Both the suction and motive fluids are assumed to be dry steam. As a result of the low pressure created at the exit of the supersonic motive steam nozzle, a suction steam is entrained to be mixed with the motive steam where both flows continue flowing towards the ejector exit. Mass ratio of suction to motive flows is a vital parameter to enhance the ejector performance. The objective of the present study is to maximize the steam ejector efficiency by optimizing the ejector mass ratio. The effect of three different geometrical parameters on ejector mass ratio and its efficiency is investigated at constant operating conditions. These parameters are the ejector convergent section angle, the length of the constant area mixing chamber and the ejector divergent section angle. The theoretical model is formulated based on single phase (superheated steam), two-dimensional and compressible flow using the finite volume solver, FLUENT 6.3. In addition, steady, axisymmetric horizontal ejector is considered. The realizable $k-\varepsilon$ model is used to model turbulence in the present simulation. The proposed numerical model is validated with the available experiments in literature. The results showed that the ejector wall static pressure distributions were greatly affected by the three investigated geometrical parameters. Furthermore, at constant operating conditions (motive, suction and back pressures) separation in the ejector divergent section started to take place at 10° at β=4.8°. In order to avoid separation, the ejector divergent section angle must be selected carefully together with the operating conditions. The ejector mass ratio and efficiency increased with increasing the previously stated three geometrical parameters to gain there upper limit values, subsequent to that, the efficiency and mass ratio decreased with increasing these geometrical parameters. Moreover, it is finally concluded that there are certain optimum ejector convergent, divergent angles and the length of the constant area mixing chamber in order to optimize the ejector mass ratio and consequently its efficiency at given constant operating condition.

KEY WORDS

Steam Ejector, Mass Ratio, Ejector Efficiency, CFD, Geometrical Parameters.

---

[1] Lecture, Dept. of Mech. Power Engineering, Faculty of Engineering, Menoufia University, Shebin El-Kom, Egypt.

[2] Professor, Dept. of Mech. Power Engineering, Faculty of Engineering, Menoufia University, Shebin El-Kom, Egypt.

INTRODUCTION

Ejectors are generally used in several applications due to their easy construction and simple operation. A highly pressurized motive steam in the ejector is known as the primary fluid. The primary fluid flows through a motive flow nozzle to entrain the secondary fluid. The primary and secondary flows mix together in a duct and then the flow pressure is recovered in a diffuser. Theoretically, there must be a complete swap of momentum at the end of mixing duct producing a uniform mixed stream flow travelling at a mean velocity between the motive and suction flow velocities. A diffuser is fitted in order to reduce the losses as possible by decreasing gradually the flow velocity to convert the exit kinetic energy from the mixing duct to pressure. Through the past decades, computational fluid dynamics (CFD) methods have been regarded as an efficient means to analyze ejector performance and to predict its behavior. A number of CFD studies were performed to investigate the effluence of ejector geometry on its performance, namely the motive nozzle exit position (NXP), the area ratio of nozzle throat to constant area section, and the length of constant area section before and after the throat [1-3]. These studies showed that the ejector performance depended greatly on the first two parameters however the third parameter slightly affected its performance.

Tarek A. Ghonim, [4] presented a comprehensive optimization of air ejectors at different and wide ranges of operating conditions and geometries. However, that previous work did not consider the change in both convergent and divergent angles of the ejector mixing duct and diffuser. Different optimum design correlations were deduced at given ejector angles to maximize the ejector efficiency and it was concluded that the entire optimization would change negatively if the ejector angles changed. Many other studies [6-9], investigated the effect of operating pressures on the performance of a steam ejector based on experimental data. They found that a decrease in the primary fluid saturated pressure caused the primary fluid mass flow to reduce. As the flow area in the mixing chamber is fixed, an increase in the secondary flow results. This caused the mass ratio of the ejector to rise. However, it caused the momentum of the mixed flow to drop. Thus, the critical pressure was reduced. On the other hand, an increase in the secondary fluid pressure, which is the ejector's upstream pressure, will increase the critical pressure. This also increased the mass flow through the mixing duct, which resulted in an increase of mass ratio. The influence of using a small primary nozzle throat diameter was similar to that of decreasing primary fluid pressure [10-13], whilst the influence of the primary nozzle exit diameter was not significant at primary fluid pressure.

The optimum geometries of two-phase flow ejector for refrigeration applications were correlated to the operating conditions by Ghonim [14]. It was stated that the maximum ejector efficiency is mainly dependent on the correct choice of the geometries which suits the operating conditions range. Computational fluid dynamics investigations were presented by Sriveerakul et al [5, 15], for predicting the steam ejector performance for refrigeration applications. They investigated the effect of operational and geometric parameters of the steam ejector on its performance and found that the ejector optimum performance is mainly governed by these parameters. Hence, justification of the ejector geometry is likely needed for optimum operation in different applications [16, 17].

The ultimate motivation behind the present work is to optimize the steam ejector efficiency by maximizing the mass flow ratio, MR at constant operating pressures. This will be fulfilled through the following:

1) Development and validation of a 2-D mathematical model to predict the performance of supersonic steam ejectors,
2) Selecting the optimum angles of the convergent mixing duct and the diffuser of an ejector in order to optimize the mass ratio for a given operating pressures,
3) Selecting the optimum constant area mixing duct length of an ejector to optimize the mass ratio for the same operating pressures as well, and
4) Relating the ejector mass ratio and efficiency to the investigated ejector geometrical parameters by numerically based correlations deduced from the theoretical investigation to optimize the ejector design (maximum efficiency).

MATHEMATICAL MODEL

The governing equations which describe the flow behavior through the ejector are presented in this section. The theoretical model is formulated based on some assumptions such as: single phase flow, two-dimensional and compressible flow. We consider a horizontal ejector and the flow is statistically steady and axisymmetric. The working fluid of the proposed model (Water vapour) was assumed to be an ideal gas. Although the ideal gas assumption seemed to be unrealistic, it was proved by some researchers, as reported in [5], that similar results to a real gas model were obtained when the operating pressure is relatively low. The water vapour properties provided in FLUENT database are shown in Table 1. The density of the working fluid is evaluated using the ideal gas relation and other properties are defined as constants throughout the simulation.

The conservation of mass equation can be written as [18,19]:

$$\frac{\partial}{\partial x}(\rho u)+\frac{\partial}{\partial r}(\rho v)+\frac{\rho v}{r}=0 \qquad \textbf{(1)}$$

The equations for momentum conservation are:

$$\frac{\partial}{\partial x}(\rho uu)+\frac{1}{r}\frac{\partial}{\partial r}(r\rho uv)=-\frac{\partial p}{\partial x}+\frac{\partial}{\partial x}\left[\mu_{eff}\left(2\frac{\partial u}{\partial x}-\frac{2}{3}(\nabla.\vec{u})\right)\right]+\frac{1}{r}\frac{\partial}{\partial r}\left[r\mu_{eff}\left(\frac{\partial u}{\partial r}+\frac{\partial v}{\partial x}\right)\right]+\rho g+S_U \qquad \textbf{(2)}$$

$$\frac{\partial}{\partial x}(\rho uv)+\frac{1}{r}\frac{\partial}{\partial r}(r\rho vv)=-\frac{\partial p}{\partial r}+\frac{\partial}{\partial x}\left[\mu_{eff}\left(\frac{\partial u}{\partial r}+\frac{\partial v}{\partial x}\right)\right]+\frac{1}{r}\frac{\partial}{\partial r}\left[r\mu_{eff}\left(2\frac{\partial v}{\partial r}-\frac{2}{3}(\nabla.\vec{u})\right)\right]-2\mu_{eff}\frac{v}{r^2}+\frac{2}{3}\frac{\mu_{eff}}{r}(\nabla.\vec{u})+S_V \qquad \textbf{(3)}$$

Here S_U and S_V are the source terms for momentum in x and r directions, respectively, and $\nabla.\vec{u}=\frac{\partial u}{\partial x}+\frac{\partial v}{\partial r}+\frac{v}{r}$

The equation of energy conservation in statistically steady 2-D (x-r) coordinate system is

$$\frac{\partial}{\partial x}\left[u(\rho E+p)\right]+\frac{1}{r}\frac{\partial}{\partial r}\left[rv(\rho E+p)\right]=\frac{\partial}{\partial x}\left[\lambda_{eff}\left(\frac{\partial T}{\partial x}-\sum h_i J_{ix}+\left(\overline{\overline{\tau}}_{eff}.\vec{V}\right)_x\right)\right]+ \frac{1}{r}\left[r\lambda_{eff}\frac{\partial T}{\partial x}\left(\sum h_i J_{ir}+\left(\overline{\overline{\tau}}_{eff}.\vec{V}\right)_r\right)\right]+S_h \quad \textbf{(4)}$$

where, $\overline{\overline{\tau}}_{eff}$ is the turbulent shear stress tensor, $\vec{V}$ is the velocity vector and S_h is the energy source term.

In the above equation, $E=h-\frac{p}{\rho}+\frac{\left(u^2+v^2\right)}{2}$

where h is the sensible enthalpy and for compressible flows it is defined as $h=\sum_i Y_i h_i$ and $h_i=\int_T^{T_{ref}} C_{P_i}\,dT$ where T_{ref} is the reference temperature and it equals 298.15 K.

The steam ejector efficiency can be given by [20]:

$$\eta = MR.\frac{\left(h_b-h_s\right)}{\left(h_m-h_b\right)} \quad \textbf{(5)}$$

where, h_b, h_s and h_m are the enthalpies of the back, suction and motive steams respectively. MR is the mass ratio (ratio of suction to motive mass flow rates).

TURBULENCE MODELING

The realizable $k-\varepsilon$ model [18, 19, 21] is used to model turbulence in the present simulation. Moreover, it is found this model provides a superior performance of the flows involving rotation, boundary layer under strong adverse pressure gradient and separation that is likely found in steam ejectors [15, 18, 19]. The realizable $k-\varepsilon$ model differs from the standard k-ε model in two important parameters. It contains a new formulation for the turbulent viscosity. Moreover, the realizable $k-\varepsilon$ model derived a new transport equation for the dissipation rate, ε. The dissipation rate has been derived from an exact equation for the transport of the mean-square vorticity fluctuation.

The governing equations for the turbulent kinetic energy and the dissipation rate are

$$\frac{\partial}{\partial x}\left(\rho u k\right)+\frac{1}{r}\frac{\partial}{\partial r}\left(r\rho v k\right)=\frac{\partial}{\partial x}\left[\left(\mu+\frac{\mu_t}{\sigma_k}\right)\frac{\partial k}{\partial x}\right]+\frac{1}{r}\frac{\partial}{\partial r}\left[r\left(\mu+\frac{\mu_t}{\sigma_k}\right)\frac{\partial k}{\partial r}\right] + G_k+G_b-\rho\varepsilon+S_k \quad \textbf{(6)}$$

$$\frac{\partial}{\partial x}(\rho u\varepsilon)+\frac{1}{r}\frac{\partial}{\partial r}(r\rho v\varepsilon)=\frac{\partial}{\partial x}\left[\left(\mu+\frac{\mu_t}{\sigma_\varepsilon}\right)\frac{\partial\varepsilon}{\partial x}\right]+\frac{1}{r}\frac{\partial}{\partial r}\left[r\left(\mu+\frac{\mu_t}{\sigma_\varepsilon}\right)\frac{\partial\varepsilon}{\partial r}\right] + \rho C_1 S_\varepsilon-\rho C_2\frac{\varepsilon^2}{k+\sqrt{\upsilon\varepsilon}}+\mathrm{C}_{1\varepsilon}\frac{\varepsilon}{k}C_{3\varepsilon}G_b+S_E \quad \textbf{(7)}$$

In these equations, G_k represents the generation of turbulent kinetic energy due to the mean velocity gradients and G_b is the generation of turbulence kinetic energy due to buoyancy. The contribution of the fluctuating dilatation in compressible turbulence to the overall dissipation rate has been neglected. S_k and S_ε are user-defined source terms. In the above equations,

$$C_1=\max\left|0.43,\frac{\eta^*}{\eta^*+5}\right| \quad ,\eta^* \text{ is the coefficient, } \eta^*=S\frac{k}{\varepsilon}, S=\sqrt{2S_{ij}S_{ij}} \quad \textbf{(8)}$$

The strain rate tensor (S_{ij}), the notation (ij) describes the direction. When i or j =1, this case corresponding to the x-direction, i or j =2 means the r-direction.

In turbulence modeling, $\mu_t=\rho C_\mu\frac{k^2}{\varepsilon}$, $\mu_{eff}=\mu+\mu_t$

As discussed earlier, the special feature of realizable $k-\varepsilon$ model is that C_μ is not a constant, and it is calculated as:

$$C_\mu=\frac{1}{A_O+A_S\frac{kU^*}{\varepsilon}}, U^*=\sqrt{S_{ij}S_{ij}+\hat{\Omega}_{ij}\hat{\Omega}_{ij}}, \hat{\Omega}_{ij}=\Omega_{ij}-2\varepsilon_{ijk}\omega_k, \Omega_{ij}=\overline{\Omega}_{ij}-\varepsilon_{ijk}\omega_k \quad \textbf{(9)}$$

Here, $\overline{\Omega}_{ij}$ is the mean rate of rotation tensor, viewed in a moving frame with angular velocity ω_k and, $A_O=4.04$, $A_s=\sqrt{6}\cos\varphi$, $\varphi=\frac{1}{3}\cos^{-1}\left(\sqrt{6}W\right), W=\frac{S_{ij}S_{jk}S_{ik}}{\tilde{S}}$, $\tilde{S}=\sqrt{S_{ij}S_{ij}}$, $S_{ij}=\frac{1}{2}\left(\frac{\partial U_i}{\partial x_j}+\frac{\partial U_j}{\partial x_i}\right)$,

The model constants are $\mathrm{C}_{1\varepsilon}=1.44, \mathrm{C}_2=1.9, \sigma_\mathrm{k}=1.0, \text{and } \sigma_\varepsilon=1.2$

SOLUTION PROCEDURE

The finite volume solver, FLUENT 6.3 [19], is used to obtain the numerical solution of the two-dimensional axisymmetric compressible Reynolds averaged Navier–Stokes (RANS) equations in connection with the realizable $k-\varepsilon$ model for closure of the RANS equations.

The steam ejector considered in the present study is constructed of the primary nozzle and the ejector. The primary flow is strongly accelerated in the nozzle and hence the secondary flow is induced through the ejector. The physical domain,

boundary conditions, the computational domain and the main geometrical parts are the secondary inflow, mixing chamber, throat and diffuser as shown in **Fig. 1**.

The discretized equations along with the initial condition and boundary conditions are solved using the segregated solution method for the segregated solver. The conservation of mass and momentum are solved sequentially and a pressure correction equation is used to ensure the conservation of momentum and the conservation of mass (continuity equation). The generated computational mesh for the considered steam ejector simulation corresponds to the measurements of [5, 15]. The effect of grid refinement on the quality of results is tested in the present study of steam ejector, in which 6200 nodes for the first nozzle part and 16950 nodes for the second mixture part which makes a grid total number of 23150 nodes. For ideal steam flow, the saturation properties (temperature and pressure), are considered at the flow inlet. The outlet pressure boundary condition is identified at the exit. Since the flow is axisymmetric about the ejector center line, only the upper half is considered for the CFD computations.

RESULTS AND DISCUSSION

The ejector performance is mainly characterized by mass ratio and the ejector efficiency. A well designed steam ejector is the one that can deliver the maximum attainable mass ratio with higher efficiency. **Figure 2** presents the code validation based on the experimental data provided by Sriveerakul et. al [15]. It is clearly shown that the presented code is capable of predicting the ejector performance well. In addition, it shows that the mass ratio is constant with back pressure increment until a certain value; in this case it is 38.5 millibars. This value is called breakdown point. By increasing the back pressure higher than the breakdown point a reversed flow region dominated at the ejector exit. Which results in delivering the steam flow back to the suction inlet and the ejector dramatically malfunctions.

The steam ejector efficiency given in **Eqn. (5)** can be enhanced by optimizing the ejector mass ratio, MR and its operating pressures as well (motive (P_m), suction (P_s) and back (P_b) pressures). M. S. Farag, [20] enhanced the ejector efficiency up to 55% by operating it at low pressure ratios for a given ejector geometry. However, present results concern with enhancing the steam ejector efficiency by optimizing its mass ratio at different ejector geometries. A motive flow nozzle with throat radius of 1 mm and an exit radius of 4 mm was used in the numerical simulation. In addition, the constant-pressure mixing section length, the constant-area mixing section radius and the diffuser length were 130, 9.5, and 180 mm. respectively. While, The operating pressures P_m , P_s and P_b were given constant values of 2.7, 0.06, and 0.075 bar respectively as well.

The effect of the constant-pressure mixing section half angle, β on the wall static pressure distribution along the ejector axis is shown in **Fig. 3**. It can be observed clearly in the figure that increasing the constant-pressure mixing section half angle leads to an increase in the static pressure along the ejector mixing sections. No abrupt pressure rise is seen in the diffuser section as a pressure outlet boundary condition is set at the exit. The increase in the static pressure at the ejector inlet may be attributed to the increase in the secondary flow suction area due to increasing the constant-pressure mixing section angle while keeping its length and exit diameter

constants. Increasing the secondary flow suction area will consequently decrease the flow velocity and increase its pressure. For a given constant-pressure mixing section half angle, the pressure is decreased up to the exit of the constant-pressure mixing section. This decrease in pressure is due to the decrease of the flow area along the ejector axis and friction as well which dominated the tendency for pressure rise caused by the mixing process itself. Furthermore, in the constant-area mixing section the static pressure increases up to a certain distance and decreases after it for almost all values of the angles, β. The increase in the pressure may be explained by the mixing process which is still taking place. However, after completion of the mixing process, the static pressure decreases only due to friction. **Figure (4)** illustrates the effect of the constant-pressure mixing section half angle, β on the centerline Mach number distribution along the ejector axis. No effect of the angle β is surely noticed along the axis of the primary flow supersonic nozzle and a very slight effect is seen in the constant-pressure mixing section. This is apparently because the mixing process is still at the beginning which means that only primary flow exits in the flow core. Moreover, after the onset of the mixing process in the constant-area mixing section it is seen that the effect of the angle β is opposite to that in **Fig. 3**. Increasing the flow Mach number will lead to an increase in the flow velocity and a decrease in its pressure. The ejector mass ratio, MR and consequently its efficiency are greatly affected by constant-pressure mixing section half angle, β which is depicted in **Fig. 5**. An optimum value of the mass ratio took place at about $\beta = 4.8^{o}$ leading to a maximum efficiency of about 10.96.

Furthermore, the influences of the constant-area mixing section length, L_{CA} on both wall static pressure and Mach number distributions along the ejector axis are illustrated respectively in **Figs. 6, and 7**. Generally, decreasing the constant-area mixing section length caused the static pressure to increase due to lesser friction except for L_{CA} =50 mm. This is apparently because for L_{CA}=50 mm the constant-area mixing section length was not long enough to complete mixing of the primary and secondary flows. **Figure 8** depicts the effect of the constant-area mixing section length on both ejector efficiency and mass ratio. Both maximum efficiency and mass ratio took place at L_{CA} =70 mm.

On the other hand, the effect of diffuser section half angle, α on the wall static pressure distribution along the ejector axis is shown in **Fig. 9**. It is shown clearly that increasing the diffuser half angle, α leads to an increase in the static pressure along the ejector axis due to an increase in the flow area except at the exit which is set as a boundary condition. Almost an opposite effect of the diffuser angle on the centerline Mach number distribution along the ejector length is reasonably shown in **Fig. 10**. The mass ratio is apparently affected by the diffuser angle which is depicted in **Fig. 11**. An optimum value of the mass ratio took place at about 3.6^{o} of the diffuser half angle. It is important to determine the optimum angle of the diffuser at a given operating condition for optimum efficiency of the ejector. Otherwise, the un-optimized diffuser angle will consequently lead to a diminished value of both ejector efficiency and mass ratio.

Comparisons between the numerically predicted ejector mass ratio and efficiency and the values obtained by the deduced correlations are illustrated respectively in **Figs. 12 and 13**. The comparisons show acceptable agreements. The numerical predictions of both ejector mass ratio and efficiency which are shown in **Figs. 5, 8**

and 11 are separately used to develop correlations relating ejector mass ratio and efficiency to constant-pressure mixing section half (β), constant-area mixing section length (L_{CA}) and diffuser section half angle (α) while keeping all operating parameters as constants. The obtained correlations for the steam ejector under consideration are in the following form:

$$Y = \sum_{k=0}^{n} a_k \, x^k \qquad \textbf{(10)}$$

where the different Coefficients, a_k are given in **Tables (2, 3 and 4)**. The correlations are valid only for the ranges shown in **Figs. 5, 8 and 11**. **Figure 14** depicts the contours of velocity streamline along the ejector axis. Severe separation is clearly seen starting from the beginning of the diffuser section which may be the reason of the decrease in efficiency shown in **Fig. 11** at $\alpha = 10^o$.

CONCLUSION

The present paper presents an optimization study for testing a steam ejector working at given operating conditions. The proposed CFD code agreed well with the available previously published experiments. The results leaded to concluding that, there are operational and geometrical constraints for using the steam ejectors in order to optimize their performances. For instance, it is important to determine the optimum angle of the diffuser at a given operating condition for optimum efficiency of the ejector. Otherwise, the un-optimized diffuser angle will consequently lead to smaller value of mass ratio.

Moreover, An optimum value of the ejector efficiency and mass ratio took place at about β=4.8^o, L_{CA}= 70 mm and α=3.6^o at given operating conditions which means that for every operating conditions range there is an optimum geometry that should be selected properly. Correlations for ejector optimum efficiency and mass ratio design were obtained by fitting the numerical results and relating these optimum values to three ejector geometric parameters, (β, L_{CA} and α). Finally, the results leaded to better understanding of the mixing process in the ejector and the phenomenon of its operation.

REFERENCES

[1] K. Pianthong, W. Sheehanam, M. Behnia, T. Sriveerakul and S. Aphornratana, “Investigation and improvement of ejector refrigeration system using computational fluid dynamics technique”, Energ. Convers. Manage. Vol. 48 (9), pp. 2556-2564 (2007).

[2] E. Rusly, L. Aye, W. S. Charters and A. Ooi, “CFD analysis of ejector in a combined ejector cooling system”, Int. J. Refrig. Vol. 28 (7), pp. 1092-1101 (2005).

[3] S. Varga, A.C. Oliveira, B. Diaconu, “Influence of geometrical factors on steam ejector performance-A numerical assessment”, Int. J. Refrig. Vol. 32 (7), pp. 1694-1701(2009).

[4] N. I. Hewedy, M. H. Hamed, F. Sh. Abou-Taleb, and T. A. Ghonim, "Optimal Performance and Geometry of Supersonic Ejector," ASME J. Fluids Eng., Vol. 130, Issue 4, pp. 41204 (2008).
[5] T. Sriveerakul, S. Aphornratana, K. Chunnanond, "Performance prediction of steam ejector using computational fluid dynamics: Part 1. Validation of the CFD results", International Journal of Thermal Sciences Vol. 46, pp.812-822 (2007).
[6] S. Varga, A.C. Oliveira, B. Diaconu, Numerical assessment of steam ejector efficiencies using CFD, Int. J. Refrig. Vol. 32 (6), pp. 1203-1211(2009).
[7] Zhang Qi, Huo Jiepeng, Liu Ruofei, Wang Ruwu, Numerical simulation and performance study of steam ejector using CFD, Int. J. Advanced Science Letters, Vol. 4, pp. 2276-2280 (2011).
[8] S.B. Riffat, S.A. Omer, CFD modeling and experimental investigation of an ejector refrigeration system using methanol as the working fluid, International Journal of Energy Reservation Vol. 25, pp. 115-128 (2001).
[9] H. J. Li., S. Q. Shen, Effect of Mixing Chamber Structure on a Steam Ejector Performance, in: the Fifth International Conference on Fluid Mechanics, Aug.15-19, Shanghai, China (2007).
[10] N. Deberne, J. F. Leone, A. Duque and A. Lallemand "A Model For Calculation Of Steam Injector Performance"; International Journal of Multiphase Flow ، Vol.25, PP.841-855 (1999).
[11] R. Yapıcı and H. K. Ersoy "Performance Characteristics of The Ejector Refrigeration System Based on The Constant Area Ejector Flow Model"; Energy Conversion and Management, Vol. 46, pp.3117-3135 (2005).
[12] S. Aphornratana "Theoretical Study of A Steam - Ejector Refrigerator"; International Energy Journal, Vol.18, No.1, pp.61-73 (1996).
[13] D. Sun "Variable Geometry Ejectors And Their Applications In Ejector Refrigeration Systems"; Energy ,Vol. 21, No. 10. pp. 919-929 (1996).
[14] T. A. Ghonim "Two-phase flow (gas-liquid) through ejectors", Ph. D. thesis in Mech. Power Eng. Dept., Menoufia University (2014).
[15] T. Sriveerakul, S. Aphornratana, K. Chunnanond, Performance prediction of steam ejector using computational fluid dynamics: part 2. Flow structure of a steam ejector influenced by operating pressures and geometries, Int. J. Therm. Sci. Vol. 46 (8), pp. 823-833 (2007).
[16] S. Aphornratana, I.W. Eames," A small capacity steam-ejector refrigerator: experimental investigation of a system using ejector with movable primary nozzle", International Journal of Refrigeration 20 (5) ,352–358 (1997).
[17] K. Chunnanond, S. Aphornratana, An Experimental investigation of a steam ejector refrigerator: the analysis of the pressure profile along the ejector, Applied Thermal Engineering, Vol. 27, pp. 311-322 (2004).
[18] Jun-De Li, "CFD simulation of water vapour condensation in the presence of non-condensable gas in vertical cylindrical condensers", International Journal of Heat and Mass Transfer, Vol.57, pp. 708-721 (2013).
[19] Ansys Fluent 16 theory's guide (2014).
[20] M. S. Farag "A numerical study for predicting steam ejector performance at different pressure ratios", 17th International Conference on Aerospace Sciences & Aviation Technology (ASAT 17) – Military Technical College, Cairo, EGYPT, April 11 - 13 (2017).
[21] T.H. Shih, W.W. Lou, A. Shabbir, Z. Yang, J. Zhou, A new k–e eddy viscosity model for high Reynolds number turbulent flow-model development and validation, Comput. Fluids, Vol. 24 (3), pp. 227-238 (1995).

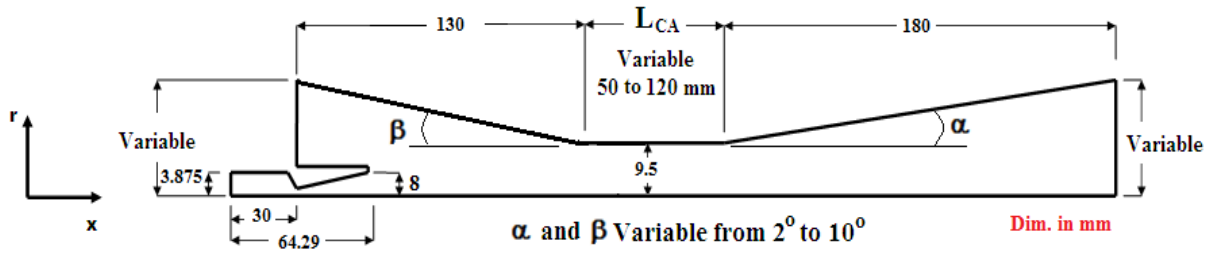

(a) Schematic drawing of the physical domain.

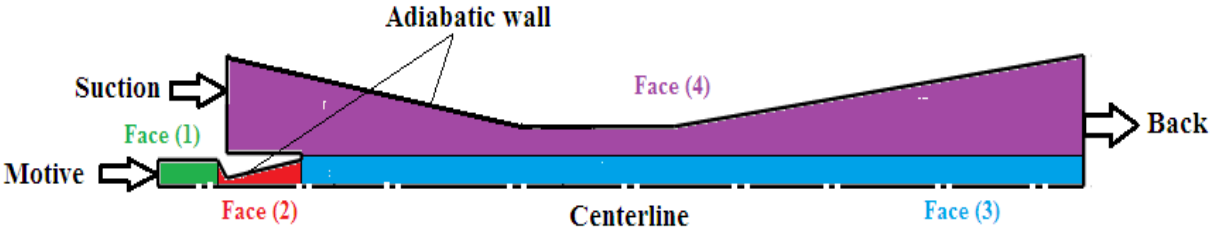

(b) Boundary conditions and the computational domain.

Fig.1. Diagram of the schematic drawing of the physical domain, boundary conditions and the computational domain for the steam ejector.

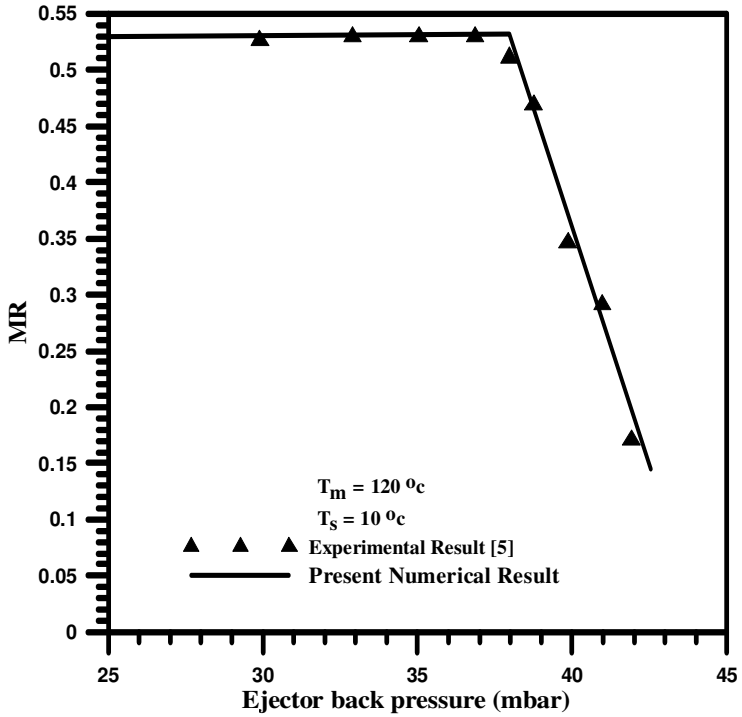

Fig. 2. Effect of back pressure on mass ratio of steam ejector based on experimental data provided by Sriveerakul et al. [5].

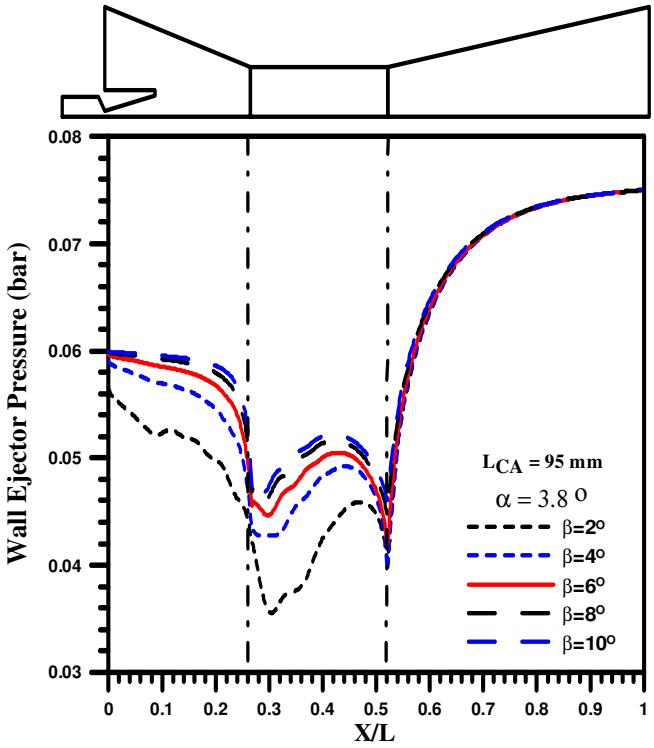

Fig. 3. Effect of constant-pressure mixing section half angle on wall static pressure distribution along the ejector axis.

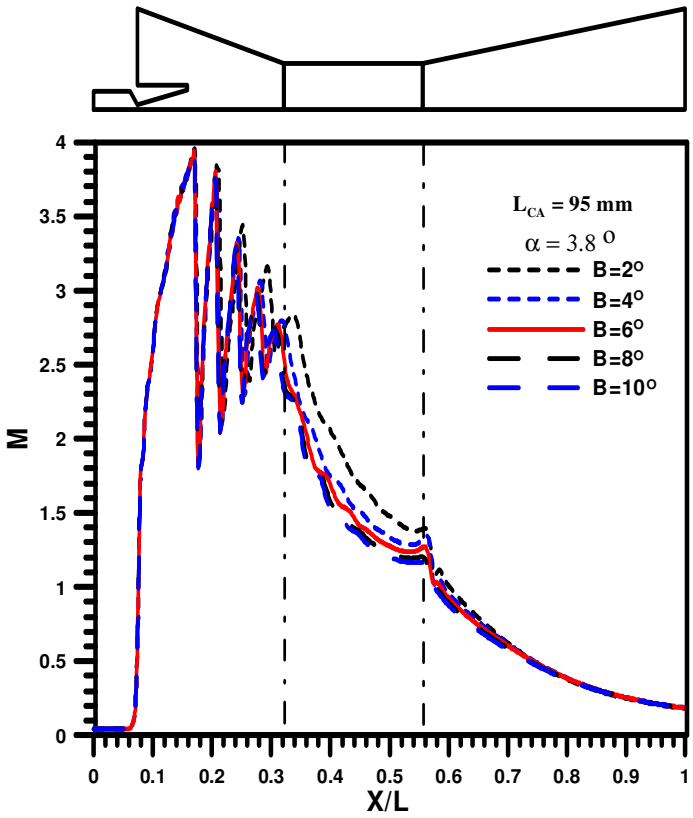

Fig. 4. Effect of constant-pressure mixing section half angle on centerline Mach number distribution along the ejector axis.

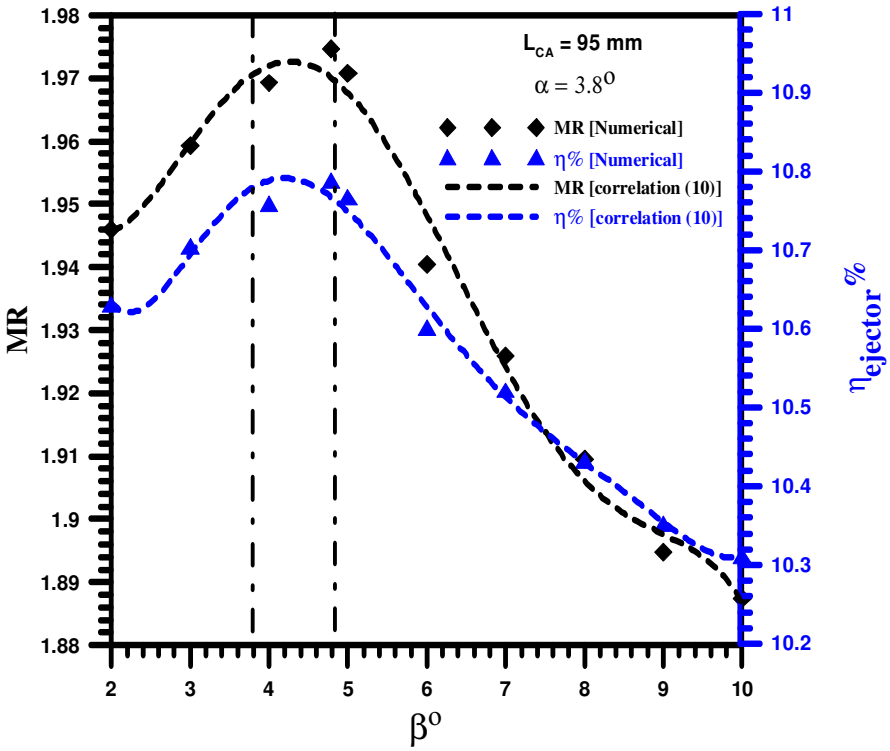

Fig.5. Effect of constant-pressure mixing section half angle on mass ratio and ejector efficiency.

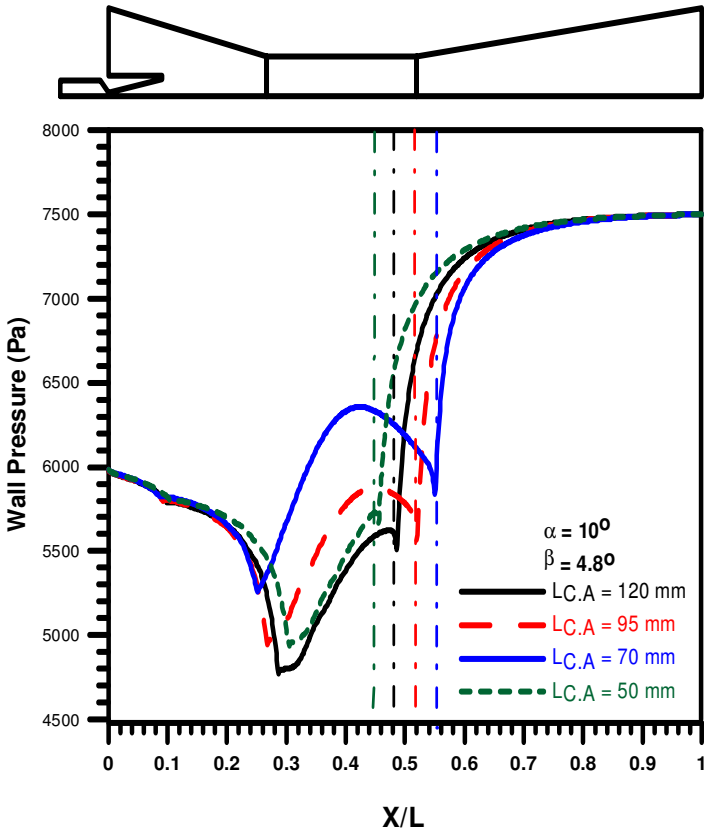

Fig.6. Effect of constant-area mixing section length on wall static pressure distribution along the ejector axis.

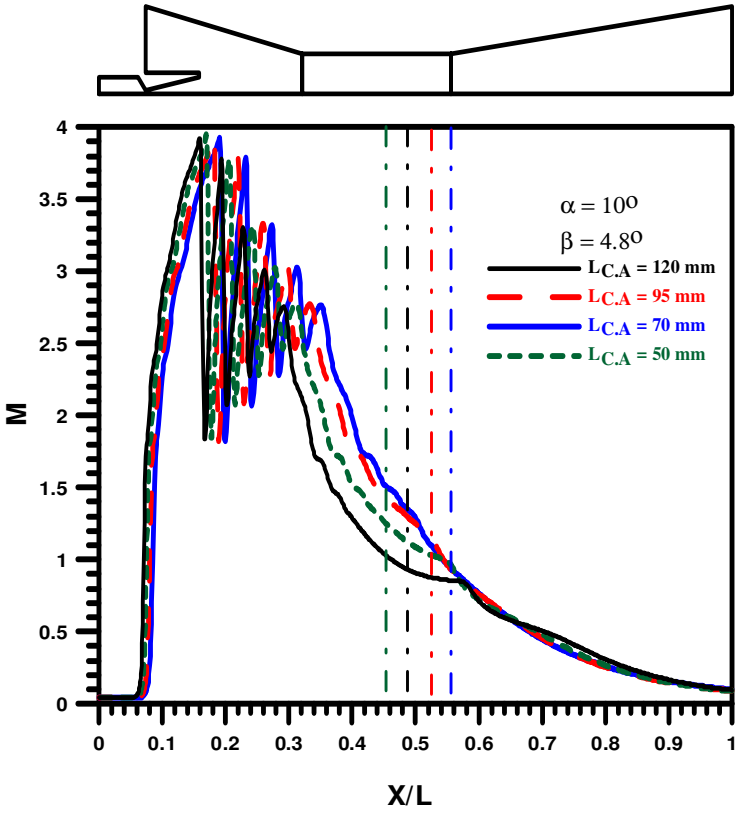

Fig. 7. Effect of constant-area mixing section length on centerline Mach number distribution along the ejector axis.

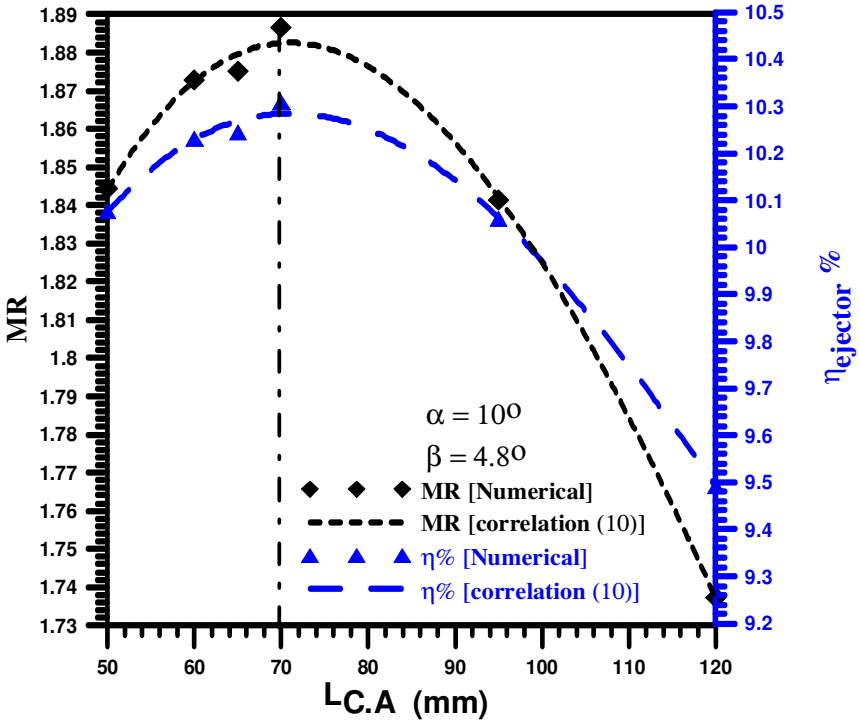

Fig.8. Effect of constant-area mixing section length on mass ratio and ejector efficiency.

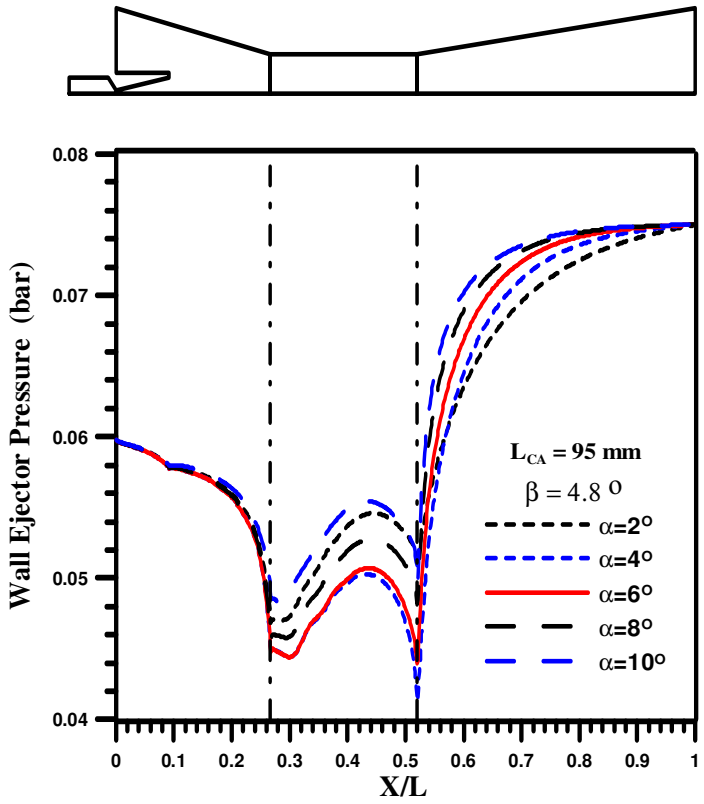

Fig. 9. Effect of diffuser section half angle on wall static pressure distribution along the ejector axis.

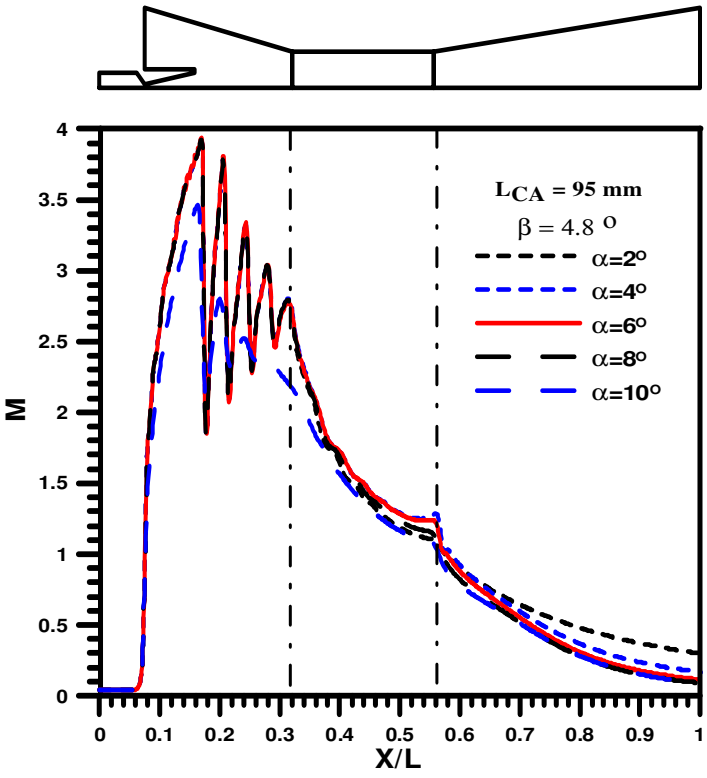

Fig.10. Effect of diffuser section half angle on centerline Mach number distribution along the ejector axis.

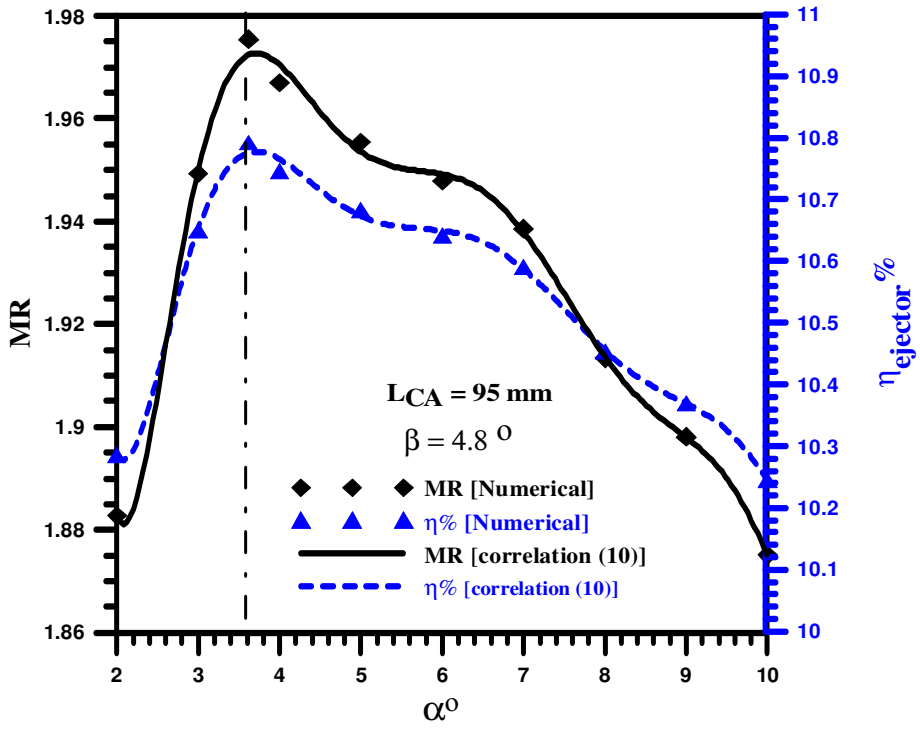

Fig.11. Effect of diffuser section half angle on mass ratio and ejector efficiency.

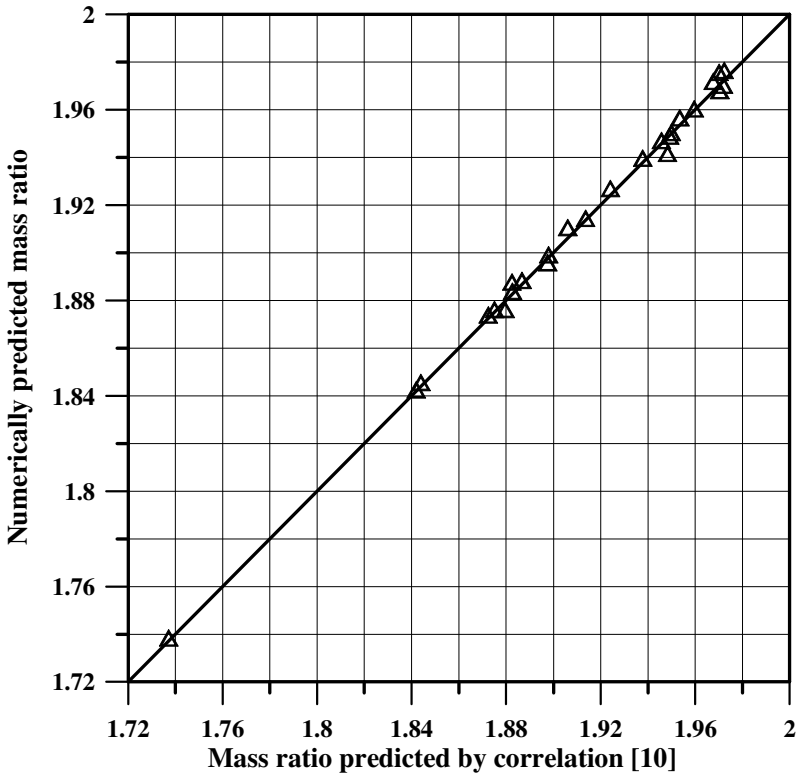

Fig.12. Comparison between numerically predicted mass ratio and values predicted by correlation (10).

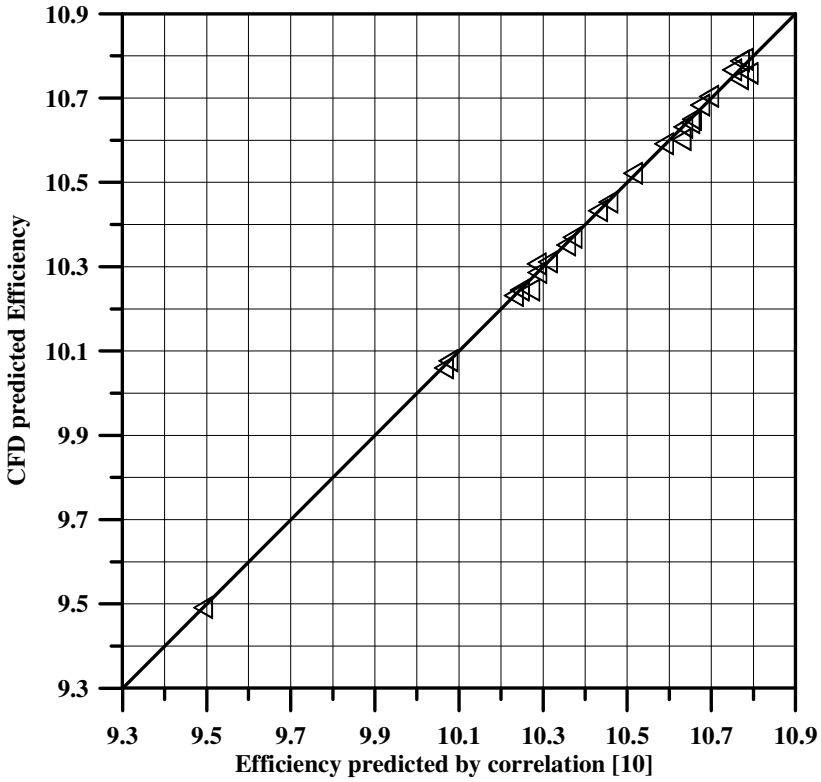

Fig.13. Comparison between numerically predicted efficiency and values predicted by correlation (10).

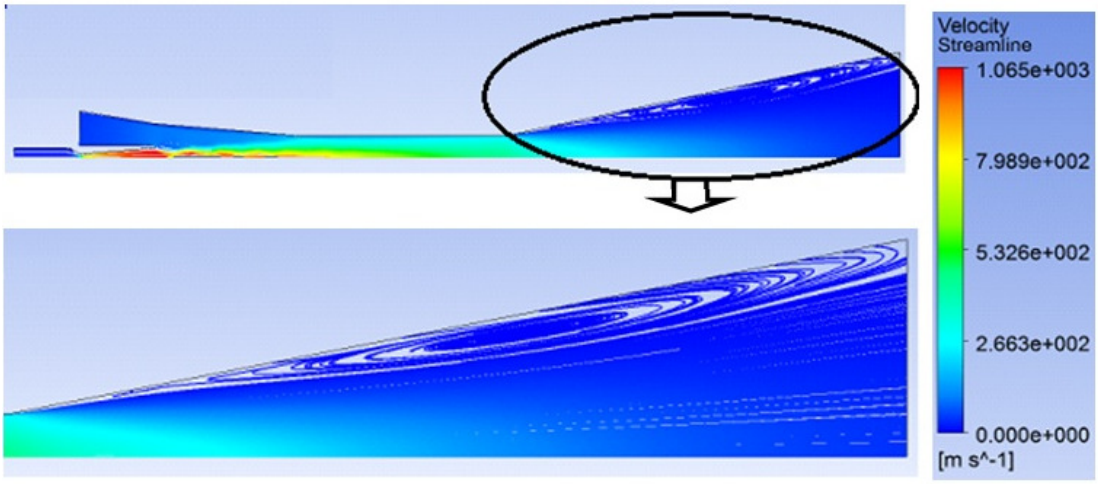

Fig.14. Contours of velocity streamlines of steam ejector at β=4.8°, L_{CA}=70 mm, and α=10°.

Table 1. Properties working fluid (water vapor) used in the CFD simulation.

Properties	Values
Viscosity, μ	1.34×10^{-5} kg/m. s
Thermal conductivity, K	0.0261 W/m. K
Specific heat capacity, Cp	2014.00 J/kg. K
Molecular weight, M	18.01534 kg/ kmol

Table 2. Coefficients of correlation **(10)** for x= β and Y=MR or η.

Y	MR	η
a_0	2.104998896	14.1679962
a_1	- 0.2244428883	- 4.850205352
a_2	0.1100710871	2.501127647
a_3	- 0.02264035249	- 0.6197396594
a_4	0.002036165661	0.0797232434
a_5	- 6.702299232E-5	- 0.005166207923
a_6	0.0	0.000133659926

Table 3. Coefficients of correlation **(10)** for x=L_{CA} and Y=MR or η.

Y	MR	η
a_0	1.343920018	7.342301619
a_1	0.01713102664	0.09359274581
a_2	- 0.0001619675085	- 0.0008848847282
a_3	3.876859108E-007	2.118062721E-006

Table 4. Coefficients of correlation **(10)** for x= α and Y=MR or η.

Y	MR	η
a_0	8.213063853	44.8708191130485
a_1	- 11.00818739	- 60.141549359134
a_2	7.788715772	42.5524582312353
a_3	- 2.944434984	- 16.0864705233089
a_4	0.6582662992	3.59633731947124
a_5	- 0.08987269131	- 0.491005713248295
a_6	0.007363484058	0.0402292697505226
a_7	- 0.0003326642623	- 0.0018174603539619
a_8	6.370720235E-6	3.48054563313376E-005